Additive Manufacturing 61 (2023) 103331

Contents lists available at ScienceDirect

Additive Manufacturing

journal homepage: www.elsevier.com/locate/addma

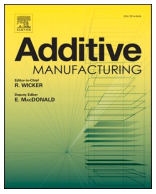

Improving fatigue performance of additively manufactured Ti-6Al-4V using sulfur-based self-terminating etching processes

Subbarao Raikar [a], Steven DiGregorio [a], Milan Agnani [b], Garrison M. Hommer [a], Owen J. Hildreth [a,*]

[a] Colorado School of Mines, Department of Mechanical Engineering, 1500 Illinois St., Golden, CO 80401, USA
[b] Colorado School of Mines, Department of Metallurgical and Materials Engineering, 1500 Illinois St., Golden, CO 80401, USA

ARTICLE INFO

Keywords:
Additive Manufacturing
Post-processing
Ti-6Al-4V
Surface Roughness
Fatigue

ABSTRACT

The adoption of Additively Manufactured (AM) Ti-6Al-4V (Ti64) is continually increasing in the industry due to its benefits over the conventional manufacturing techniques. However, AM Ti64 parts are prone to poor surface finish, which significantly affects their fatigue performance. Therefore, AM Ti64 parts need post-processing to enhance surface finish and fatigue performance. Prior work with a sulfur-based self-terminating etching process for AM Ti64 demonstrated support removal and surface roughness reduction. To further this work, this manuscript details the impact of this sulfur-based post-processing technique on the mechanical properties and the fatigue life of AM Ti64 by characterizing the surface roughness, microstructural evolution, and fracture surfaces. This post-processing technique decreased the surface roughness parameter - S_v by 55 % from 84 ± 11 μm to 38 ± 19 μm and increased the average fatigue life by 340 % from about 7000 cycles to 30,000 cycles.

1. Introduction

Additive Manufacturing (AM) of Ti-6Al-4V (Ti64) components is of great interest due to its ability to form complex geometries with less material waste, quicker turnaround times, and lower cost than conventional manufacturing processes [1]. However, AM parts are prone to poor surface finish, high residual stresses, and porosity, reducing fatigue performance [2–4]. In addition, printing process parameters such as the incident energy, powder size, and layer thickness directly affect the surface roughness [5,6]. Although researchers have improved the surface roughness by optimizing printing process parameters, additional post-processing is necessary to improve the surface finish for better fatigue performance.

Post-processing methods for surface finishing involve mechanical grinding and machining [7], laser-based [8], and chemical-based [9] treatments [10]. Mechanical surface finishing methods include mechanical machining, ultrasonic nanocrystal surface modification (UNSM), and the use of abrasives [10]. Fatemi et al. showed that improving the surface finish of AM Ti64 by machining improved the fatigue performance compared to that of as-printed specimens [11]. Zhang et al. showed the use of UNSM and electrically assisted UNSM to improve the fatigue performance of AM Ti64 [12,13]. Ma et al. improved the surface finish of AM Ti64 by using laser polishing, and the microstructural changes due to this process also lead to higher wear resistance [14]. While the above-mentioned deformation-based post-processing techniques and laser polishing can effectively decrease the surface roughness, they cannot be used to process complex geometries with inaccessible internal surfaces. Presenot et al. used a solution of hydrofluoric acid, nitric acid, and deionized water to chemically polish AM Ti64 to improve the surface finish. This resulted in a 60 % increase in the fatigue strength of the chemically polished AM Ti64 compared to as-printed specimens [15]. While chemical polishing can improve the surface finish of parts with fluid-accessible internal surfaces, the process is often non-uniform since the concentration of the etchant decreases as the fluid moves from the leading surfaces compared to the trailing surfaces.

To address these post-processing issues, the Hildreth group recently introduced a sulfur-based Self-Terminating Etching Process (STEP) for AM Ti64 that not only improves the surface finish but can also be used for support removal [16]. In this process, elemental sulfur gas reacts with the top ~50 μm of the surface of AM Ti64 to form the respective sulfides at 950 °C. Then, a sulfuric acid and sodium molybdate solution

Abbreviations: AM, Additive Manufacturing; Ti64, Ti-6Al-4V; STEP, Self-Terminating Etching Process; SLM, Selective Laser Melting.

* Corresponding author.
E-mail address: ohildreth@mines.edu (O.J. Hildreth).

https://doi.org/10.1016/j.addma.2022.103331
Received 23 June 2022; Received in revised form 25 October 2022; Accepted 26 November 2022
Available online 1 December 2022

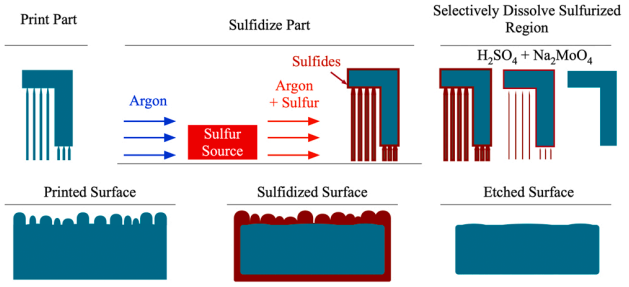

Fig. 1. Schematic of the sulfur-based self-terminating etching process for support removal and surface finishing of AM Ti64.

Table 1
Composition of Ti-6Al-4V powder by EOS.

Composition	wt%
Al	5.50–6.75
V	3.50–4.50
O	≤ 0.2
N	≤ 0.05
C	≤ 0.08
H	≤ 0.015
Fe	≤ 0.30
Y	≤ 0.005
Other elements	≤ 0.4
Ti	Balance

selectively etches the sulfides at room temperature while protecting the base Ti64. Fig. 1 shows a schematic of the STEP and its effect on the surface. Since each sulfidation-etching cycle removes ~50 μm of Ti64, multiple cycles are required to dissolve thicker supports [16]. The sulfidation process is diffusion limited, i.e., the reaction between sulfur gas and Ti64 leads to the formation of a sulfide layer that grows in thickness as the reaction proceeds. The sulfide layer growth rate decreases as the sulfide scale thickness increases, leading to the formation of a uniform sulfide layer on all the surfaces of Ti64, particularly in high-aspect ratio parts like internal channels. During the etching process, only the uniform sulfide layer is dissolved in a self-terminating manner that protects the integrity Ti64 under the sulfide scale. Thus, leading to uniform amount of material removed from all the surfaces, internal and external.

While support removal and surface finishing demonstration showed the potential of this novel sulfidation and etching process, the mechanical properties and fatigue performance of Ti64 after processing using this sulfur-based post-processing have not been studied. These properties are a critical metric when evaluating any AM post-processing technique. This work fills this information gap by studying the impact of the sulfur-based post-processing technique on the tensile properties and fatigue performance of AM Ti64. Here, the mechanical properties, including the cycles to failure, surface roughness, microstructure, and fracture surfaces, are compared for fatigue specimens in as-printed condition, as-printed heat-treated without any surface finishing, and after the sulfur-based post-processing. These results show that this sulfur-based process improves the fatigue performance of printed Ti64 specimens by at least 3 × because of the microstructural evolution and the improvement in surface finish.

2. Materials and methods

2.1. Specimen preparation

Ti64 tensile and fatigue specimens with circular cross-sections and the block with an internal channel were fabricated using an EOS M 290 printer. Fig. S1 in the Supporting Information shows the drawing and dimensions of the tensile and fatigue specimens and their printing orientation. The specimens' fabrication conditions were as follows: 30 μm layer thickness with laser power of 280 W, speed of 1200 mm/s, and hatch spacing of 0.14 mm. The composition of the Ti64 powder, as stated by the powder manufacturer (EOS), is listed in Table 1.

Table 2
Specimen process condition and the tests performed with the respective condition.

Specimen Condition	Surface Finishing	Heat Treatment	Tensile	Fatigue
As-printed	No	No	Yes	Yes
As-printed heat-treated	No	Yes	No	Yes
STEP with sulfur and iodine	Yes	Yes	Yes	Yes
STEP with sulfur only	Yes	Yes	No	Yes

The printed specimens were cleaned in an ultrasonic bath with deionized (DI) water (18.2 MΩ, Thermo Scientific Smart2Pure), acetone, methanol, and isopropyl alcohol for 5 min each sequentially. After ultrasonication with each solvent, the specimens were dried with compressed N_2 to remove any excess solvent. Then, STEP is performed on the cleaned specimens. Since its initial development, STEP has been modified to eliminate sub-surface sulfidation, reduce the number of cycles for support removal, and decrease the cycle time for faster processing. Firstly, decreasing the sulfidation temperature from 950 °C to 750 °C eliminated sub-surface sulfidation. Sulfidation in the presence of iodine led to an increase in the amount of Ti64 consumed per cycle of sulfidation and reduced the number of cycles required for support removal. Finally, etching at 80 °C led to an increase in the etch rate and effectively decreased the cycle time. However, after noticing detrimental effects on the surface finish, sulfidation in the presence of iodine and etching at 80 °C were discontinued.

Table 2 shows the specimen process conditions and the tests performed in this work. Tensile tests were conducted with as-printed and STEP with sulfur and iodine specimens. Fatigue tests were conducted with all four conditions. The as-printed condition refers to the specimens that have not undergone any post-processing after the printing process. The as-printed heat-treated condition refers to the specimens subjected to the thermal processing of the STEP specimens without any surface finishing effects. These specimens were prepared by encapsulating as-printed specimens in fused quartz without any sulfur or iodine and subjected to the same heat treatment cycles as the STEP specimens. The procedure and process history of STEP with sulfur and iodine and STEP with sulfur only specimens are described in the following subsection.

2.2. Self-terminating etching process

Sulfur and iodine were carried into a tube furnace (Lindberg HT55342C) through a static inline mixer (Model No.1/4–40–3–12–2, Koflo Corporation) with the help of argon (99.999 %, General Air) flow through a bubbler of sulfur flakes (≥ 99.99 % trace metals basis, Sigma-Aldrich) at 150 °C and an iodine (≥ 99.99 % trace metals basis, Sigma-Aldrich) bubbler at room temperature. The argon flow rates were adjusted such that the gas mixture contained one percent of iodine by volume. Specimens were sulfidized in the tube furnace at 750 °C for 12 h, and the specimens were water quenched. The iodine bubbler was disconnected for STEP with a sulfur-only cycle, and a fresh mullite tube was used. The specimens were etched in a solution of 5 M sulfuric acid (H_2SO_4, 95–98 %; VWR Chemicals) and 0.25 M sodium molybdate (Na_2MoO_4, ≥ 98 %, Sigma-Aldrich). Fig. S2 in the Supporting Information shows the setup for sulfidation using a tube furnace.

A set of six cleaned specimens, one set each of fatigue and tensile specimens, were subjected to STEP with sulfur and iodine for three cycles at 750 °C and etched at 80 °C to accelerate the etching process. Fig. 2a shows the poor surface after the first three cycles of sulfidation and etching. The poor surface finish could be attributed to the aggressive effect of iodine on material consumption. Therefore, the use of iodine

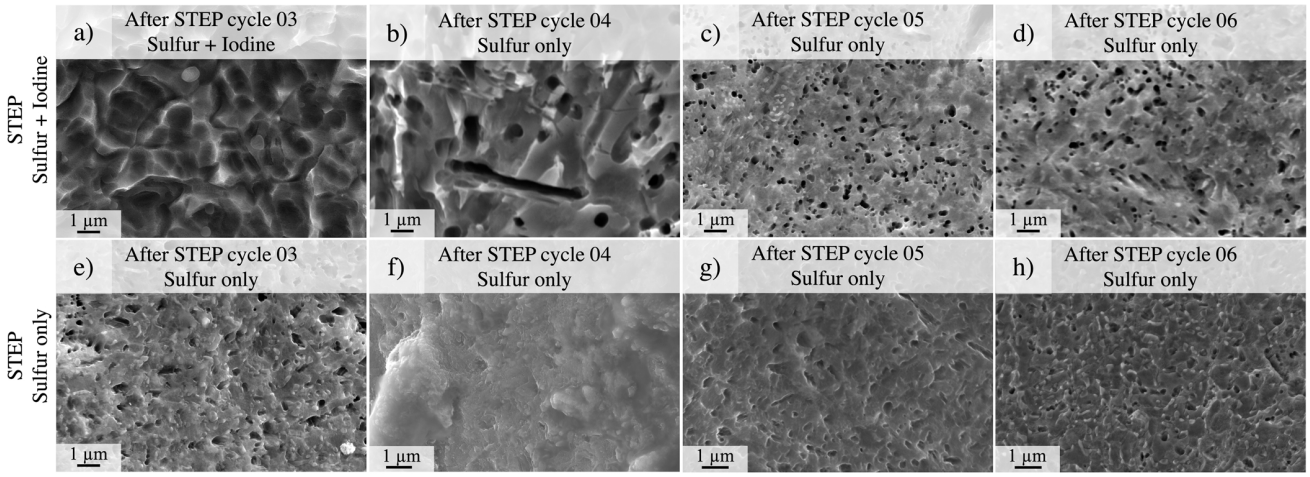

Fig. 2. SEM images of the surface evolution of one specimen each from STEP with sulfur and iodine (top row) and STEP with sulfur (bottom row) after a) and e) cycle 03, b) and f) cycle 04, c) and g) cycle 05 and d) and h) after cycle 06 respectively. Figures a) and b) show the sharp features due to the detrimental effect of iodine and etching at 80 °C. These features are absent in the STEP with sulfur specimens and room temperature etching.

Table 3
STEP parameters for sulfidation and etching of STEP with sulfur and iodine specimens.

	Sulfidation Temperature [°C]	Sulfidation Duration [hr]	Sulfidation Enclosure	Iodine	Etching Temperature [°C]
Cycle 01	750	12	Tube furnace	Yes	80
Cycle 02	750	12	Tube furnace	Yes	80
Cycle 03	750	12	Tube furnace	Yes	80
Cycle 04	750	12	Tube furnace	No	80
Cycle 05	750	4	Quartz encapsulation	No	22
Cycle 06	750	4	Quartz encapsulation	No	22

Table 4
STEP parameters for sulfidation and etching of STEP with sulfur only specimens.

	Sulfidation Temperature [°C]	Sulfidation Duration [hr]	Sulfidation Enclosure	Iodine	Etching Temperature [°C]
Cycle 01	750	4	Quartz encapsulation	No	22
Cycle 02	750	4	Quartz encapsulation	No	22
Cycle 03	750	4	Quartz encapsulation	No	22
Cycle 04	750	4	Quartz encapsulation	No	22
Cycle 05	750	4	Quartz encapsulation	No	22
Cycle 06	750	4	Quartz encapsulation	No	22

was discontinued for following sulfidation cycles. For the fourth cycle, the fatigue specimens were subjected to STEP with sulfur only in the tube furnace at 750 °C for 12 h and etched at 80 °C. However, the surface finish of the specimens after the first four cycles was poor, with sharp features that can be detrimental to the fatigue performance, as shown in Fig. 2b. Therefore, etching at 80 °C was also discontinued. Hereafter, the specimens were subjected to two STEP cycles with only sulfur in a fused quartz tube to minimize the effect of uncertainties and nuisance factors associated with the tube furnace setup. A representative fused quartz encapsulation is shown in Fig. S3 in the Supporting Information as a visual aid. The encapsulated specimens were sulfidized in a box furnace at 750 °C for 4 h and water quenched. The specimens were then etched at room temperature. The surface finish improved with sulfur-only cycles, as shown in Fig. 2c and d.

To eliminate the potentially detrimental effect of iodine and etching at 80 °C, another set of six as-printed fatigue specimens was encapsulated in a fused quartz tube individually with 50 mg sulfur only, for each STEP cycle, to avoid the sharp features seen with the previous set of specimens. Fig. 2e, f, g, and h show the surface of the fatigue specimens after the third, fourth, fifth, and sixth cycles of STEP with sulfur. These surfaces do not show any sharp features, such as those seen in Fig. 2a and Fig. 2b. Even though the final surface looks reasonably similar for both the specimens, the detrimental effects from the previous processes, i.e., STEP with sulfur and iodine and etching at 80 °C, could significantly affect the fatigue performance. The summarized process histories for both sets of specimens are tabulated in Table 3 and Table 4. The diameters of both sets of fatigue specimen decreased by ~100 μm, i.e. ~50 μm of Ti64 was removed from the surface of the specimens. The diameters and the material removed from the surface of all the fatigue specimens are plotted in Fig. S4 of the Supporting Information. Figure S5 shows the orientation of the fatigue specimen surfaces with respect to the build direction.

2.3. Mechanical testing

All the specimens were tested on an MTS Landmark 370.10 servo-hydraulic load frame with hydraulic vee wedge grips. The tension-tension fatigue specimen stress bounds were 620.5 MPa (90 ksi) and 62.1 MPa (9 ksi), as recommended by the specimen supplier. The fatigue testing with a loading ratio, R of 0.1 was conducted with a cycle frequency of 20 Hz. Quasi-static tensile testing was also performed on the MTS load frame equipped with a half-inch axial extensometer (632.26E-43, MTS) with a strain rate of 0.001 s^{-1}.

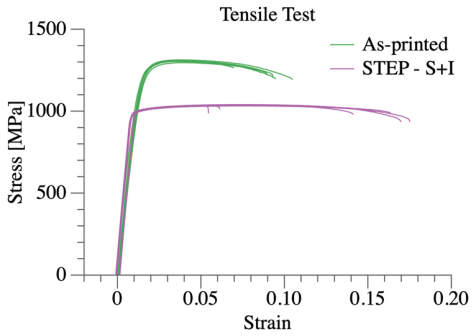

Fig. 3. Stress-Strain curves from tensile testing of six as-printed specimens and six specimens subjected to STEP with sulfur and iodine. The as-printed specimens have higher ultimate tensile strength and yield strength but lower ductility than the STEP specimens.

2.4. Characterization

Each specimen was cut into two pieces using a metallographic saw (MSX-250 M2, LECO) with an Al_2O_3 abrasive blade for roughness and microstructure data. One-half was used for radial cross-section information and the other for axial cross-section information. The specimen pieces were placed in cold-curing epoxy (EpoFix, Struers) within 1.25-inch diameter mold cups. After the epoxy cured, these samples were ground with silicon carbide paper sequentially from 180 grit to 600 grit, followed by polishing with 9 μm diamond suspension and finishing with 0.05 μm colloidal silica with 20 % v/v hydrogen peroxide (30 % H_2O_2 in water, Fisher Chemical). The samples were thoroughly rinsed with water and isopropyl alcohol and dried with compressed N_2 between each step. For microstructural analysis, the polished samples were stain-etched at room temperature using an immersion solution of ammonium bifluoride and deionized water for 60 s. 6 mm line profiles were obtained from the axial cross-section images using ImageJ [17] for surface roughness characterization. The surface profile images were then processed to obtain the coordinates on MATLAB to calculate the roughness parameters. Areal roughness parameters were obtained from three $650 \times 650\ \mu m^2$ areas using Olympus LEXT OLS5100 laser scanning microscope. The images for microstructural examination and roughness characterization were collected with light optical microscopy (Axio Vert.A1, Zeiss). The fatigue specimen surfaces and the fracture surfaces were imaged with an accelerating voltage of 15 kV on SEMTech Solutions Model 3300 Field Emission Scanning Electron Microscope.

3. Results and discussion

The STEP post-process used in this study has several advantages over other post-processing methods. First, the chemical approach allows for both external and internal surface processing. Second, the self-terminating nature facilitates more uniform material removal, even on high aspect ratio internal channels. Third, the surface roughness and microstructure enhancements can improve the fatigue performance of printed parts. This study focuses on quantifying the tensile properties and fatigue performance, and connecting it to the microstructure, surface roughness, and fracture surface for as-printed, as-printed heat-treated, after STEP with sulfur and iodine, and after STEP with sulfur only.

3.1. Tensile testing

Fig. 3 shows the stress-strain curves for specimens as printed and after STEP with sulfur and iodine. Table 3 lists the average tensile properties of the tested specimens with one standard deviation as error. The STEP tensile specimens show an overall decreased strength compared to the as-printed specimens. The elastic modulus of the as-printed specimens (102 ± 2 GPa) is slightly lower than that of the STEP specimens (115 ± 1 GPa), which could be a result of texture [18] or due to inaccuracies in the measurement of the diameter of the specimens. The difference in the measured diameter and load-bearing diameter of STEP specimens could be smaller than that of as-printed specimens due to the lower surface roughness of STEP specimens should also be noted. STEP decreased the average ultimate tensile strength (UTS) from 1305 ± 6 MPa to 1035 ± 3 MPa and decreased the yield strength (YS) from 1120 ± 11 MPa to 991 ± 6 MPa, compared to the as-printed specimens. STEP also increased the average elongation from 9 ± 1 % to 13 ± 5 % and the average toughness from 105 ± 16 MPa to 126 ± 56 MPa, compared to the as-printed specimens. A higher UTS typically suggests better fatigue performance [19]. However, lower elongation and toughness, indicating the less ductile nature of the as-printed specimens compared to the STEP specimens, can result in poor fatigue performance. Less ductile nature makes fatigue specimens prone to rapid crack initiation due to higher sensitivity to surface roughness [20]. Tensile testing was not performed for STEP with sulfur only since its thermal processing history was the same as STEP with sulfur and iodine. Micro-hardness measurements corroborate this reasoning. Vickers micro-hardness values of the as-printed heat-treated, STEP with sulfur and iodine, and STEP with sulfur are similar and lower than that of the as-printed condition, shown in the Supporting Information Fig. S2. Table 5.

Table 5
Tensile properties of as-printed and STEP with sulfur and iodine specimens.

Tensile property	As-printed	STEP – S+I
Modulus [GPa]	102 ± 2	115 ± 1
UTS [MPa]	1305 ± 6	1035 ± 3
YS [MPa]	1120 ± 11	991 ± 6
Elongation [%]	9 ± 1	13 ± 5
Toughness [MPa]	105 ± 16	126 ± 56

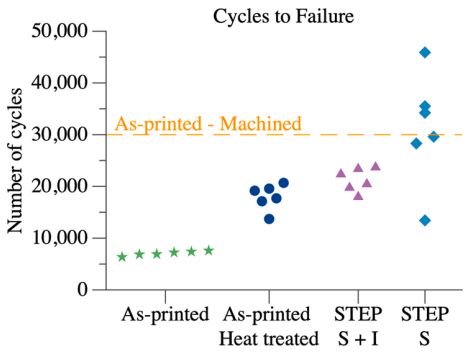

Fig. 4. Plot comparing the number of cycles to failure for as-printed, as-printed heat-treated, STEP with sulfur and iodine, and STEP with sulfur only specimens. Both the sets of STEP specimens with surface finishing outperformed the as-printed and STEP heat treatment specimens attributing the additional increase in cycles to failure to surface finishing aspect of STEP. The STEP with sulfur only specimens' cycles to failure is comparable to the cycles to failure of as-printed machined specimens (Information provided by the supplier).

3.2. Effect of STEP on fatigue life

As-printed, as-printed heat-treated, STEP with sulfur and iodine, and STEP with sulfur only fatigue specimens were tested, with a cyclic peak loading of 620.5 MPa and an R value of 0.1 with a frequency of 20 Hz, to study the effect of STEP on the fatigue performance. Fig. 4 compares the number of cycles to failure for the four specimen process conditions. The dashed orange line indicates the fatigue life of machined as-printed specimens for reference (provided by the specimen supplier). Both sets

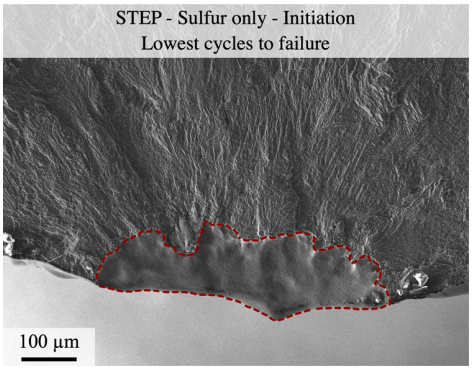

Fig. 5. Fracture surface of the STEP with sulfur fatigue specimen with the lowest cycles to failure. Compared to the rest of the STEP with sulfur specimens, the untimely fatigue failure can be attributed to the large surface defect (shown with the dotted red lines).

of STEP specimens (sulfur with iodine and sulfur only) outperformed both the as-printed specimens and as-printed heat-treated specimens, with the as-printed specimens failing at a mere ~ 7000 cycles, as-printed heat-treated specimens around ~ 18,000 cycles, STEP sulfur with iodine specimens failing around ~ 20,000 cycles, and STEP with sulfur only specimens failing around ~ 31,000 cycles. The average number of cycles to failure for STEP with sulfur-only specimens is comparable to that of machined as-printed specimens, as mentioned by the supplier. The as-printed heat-treated specimens outperform the as-printed specimens showing that the thermal cycling during the STEP process improves the fatigue performance. This is likely a result of the heat treatment since there was no change in the surface finish of the specimens after the heat treatment.

Along with the microstructural changes, the removal of detrimental residual tensile stresses that accelerate crack initiation and failure could have enhanced the fatigue performance of as-printed heat-treated specimens over as-printed specimens [21]. The fatigue performance of the STEP with sulfur and iodine specimens is comparable to that of the as-printed heat-treated specimens. The surface finishing provided by STEP with sulfur and iodine has improved the fatigue performance by ~ 2000 cycles compared to the as-printed heat-treated specimens. However, the STEP with sulfur only specimens failed after an additional ~ 20,000 cycles compared to the as-printed heat-treated specimens highlighting the influence of the surface finishing aspect of STEP. The poor performance of the STEP with sulfur and iodine specimens compared to the STEP with sulfur specimens can be attributed to the detrimental effects caused by the presence of iodine and etching at 80 °C, as discussed earlier in Section 2.2 and shown in Fig. 2. The cycles to failure data for STEP with sulfur specimens has more variance than specimens with other process conditions. In particular, the specimen with the lowest cycles to failure has a large surface defect (red dotted line), as shown in the initiation site of the fracture surface of the specimen in Fig. 5, that could have led to the untimely fatigue failure of the specimen. We investigated the specimen surface roughness, microstructure, and fracture surfaces to further understand how STEP improves fatigue performance.

3.3. Microstructural analysis

The tensile deformation behavior, crack initiation, and propagation depend on the microstructure. Fig. 6 shows the optical images of the axial stain-etched cross-sections revealing the microstructure of the as-printed, as-printed heat-treated, STEP with sulfur and iodine, and STEP with sulfur only samples. The as-printed microstructure primarily consists of fine acicular α′ martensite structures (Hexagonal Close Packed (HCP) structure) due to the high-temperature gradients inherent to the SLM process [2]. These fine structures are associated with higher strength and lower toughness, as observed with the stress-strain curves in sub-Section 3.1. The as-printed heat-treated, and both the STEP microstructures consist of α (HCP structure) lathes distributed in a β (Body-Centered Cubic (BCC) structure) matrix along with some acicular α′ structures. The α′ martensite from the printing process decomposed to a mixture of α and β [22] during STEP at 750 °C. The transformation of α and β phases from α′ during STEP explains the lower UTS and YS of the STEP tensile specimens since β is a relatively more ductile phase, and its presence decreases the strength of the material [23]. The presence of the β phase also contributes to the higher ductility observed in the STEP specimens compared to the as-printed specimens. Ductile materials are usually less sensitive to stress concentration due to surface roughness [24], and this could be one of the reasons for the better fatigue performance of STEP specimens. STEP with sulfur and iodine specimens underwent thermal processing of 750 °C for 12 h for the first three cycles, followed by three more cycles at 750 °C for 4 h.

In contrast, STEP with sulfur only specimens underwent six cycles at 750 °C for 4 h. However, the microstructures for both sample sets are identical even with different thermal processing durations. This is because both the α and the β phases tend to coarsen with longer hold times, but their growths hinder each other and limit overall grain growth [18]. Overall, the transformation of fine acicular α′ to α + β lamellar microstructure resulted in higher ductility that decreased the sensitivity to surface roughness and increased the resistance to crack propagation.

3.4. Surface roughness analysis

Surface roughness and irregularities can influence the fatigue performance of a Ti64 part since these irregularities act as primary initiation sites for cracking [25]. The surface irregularities are characterized by analyzing cross-sectional images of the surface and quantifying the surface roughness for the axial cross-sections since the cyclic loading direction is perpendicular to the surface roughness. Fig. 7 shows the

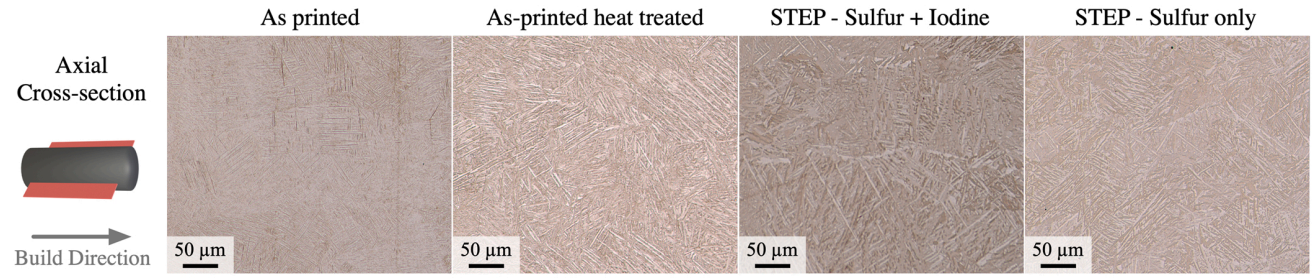

Fig. 6. Optical images of the axial stain-etched cross-sections of as printed, STEP with sulfur and iodine, and STEP with sulfur only fatigue samples. The α′ structure in the as-printed samples transforms to α + β lamellar microstructure after the heat treatment or after STEP. α-phase is lighter regions, and the β-phase is darker in the as-printed heat-treated, STEP – Sulfur + Iodine, and STEP – Sulfur only images. The orientation of the cross-section with respect to the build direction is shown in the schematic on the left.

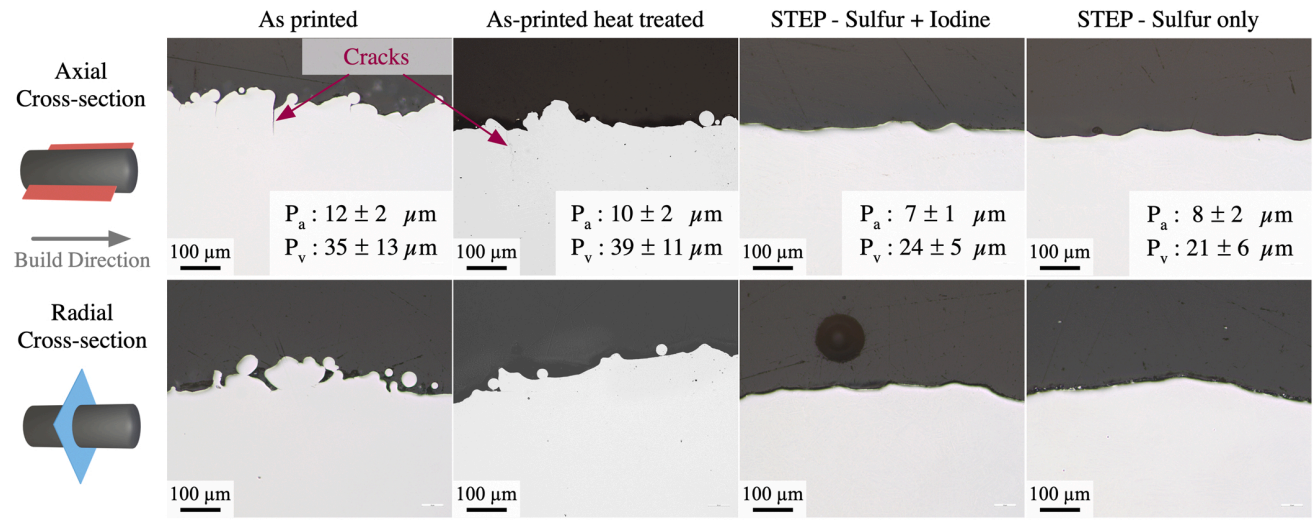

Fig. 7. Inverted microscope images of the axial and radial cross-sections of the as-printed, as-printed heat-treated, STEP with sulfur and iodine, and STEP with sulfur only with P_a and P_V values on the bottom right corner of the axial cross-sections. The balling effect and the other notch-like surface irregularities contributing to stress concentration have been removed with STEP leading to a decrease in P_v by ~33 %. The orientations of the cross-sections with respect to the build direction are shown in the schematic on the left.

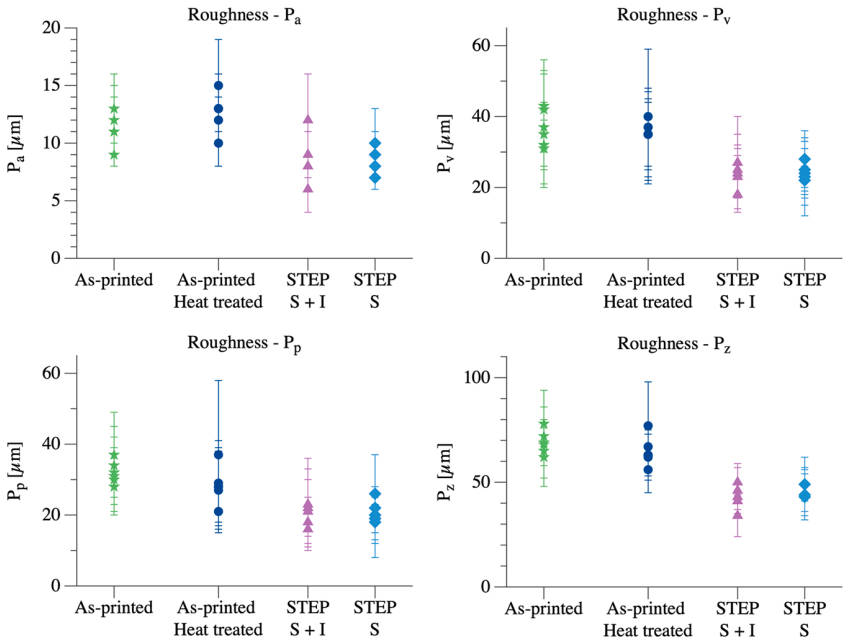

Fig. 8. Plot of average profile roughness (P_a), average minimum valley depth (P_v), average maximum peak height (P_p), and average maximum profile height (P_z) from the axial cross-sections of the fatigue samples. The samples without any surface treatment (as-printed and as-printed heat-treated samples) have a higher P_a, P_v, P_p, and P_z than the samples with surface finishing (STEP with sulfur and iodine and STEP with sulfur only). This corroborates the contribution of the surface finishing aspect of STEP towards fatigue performance.

axial and radial cross-sections of the fatigue samples with the highest cycles to failure in their respective sets. The as-printed samples have notch-like surface irregularities that act as stress concentration sites in axial and radial cross-sections. These notch-like surface irregularities and the balling effect are not present in STEP samples. The acuity of the surface features has also decreased after STEP. Cracks from the surface are observed only in the as-printed and as-printed heat-treated axial cross-sections perpendicular to the cyclic loading direction. The absence of such cracks in the STEP samples indicates that the removal of surface irregularities leads to a decrease in stress concentration and, ultimately, crack initiation sites during fatigue testing.

The surface roughness parameters, average profile roughness (P_a), average minimum valley depth (P_v), average maximum peak height (P_p), and average maximum profile height (P_z) were calculated from the 6 mm long outlines of the axial cross-sections obtained from ImageJ. The surface profiles from cross-section images were divided into five equal segments to calculate the roughness parameters for each segment since obtaining the surface profile with contact profilometry on curved surfaces would be challenging. The outlines are also more accurate than optical surface profilers since light cannot reach the region of interest when the surface irregularities cover the region of interest [26] as seen in the as-printed cross-sectional images in Fig. 7. However, the fatigue specimen surfaces have also been characterized to obtain areal roughness parameters with a laser scanning microscope in addition to the profiles from the cross-sectional images. The roughness parameters reported in Fig. 8 are the average values calculated from the five segments with one standard deviation as the error bars. The samples without any surface treatment, i.e., the as-printed and the as-printed heat-treated

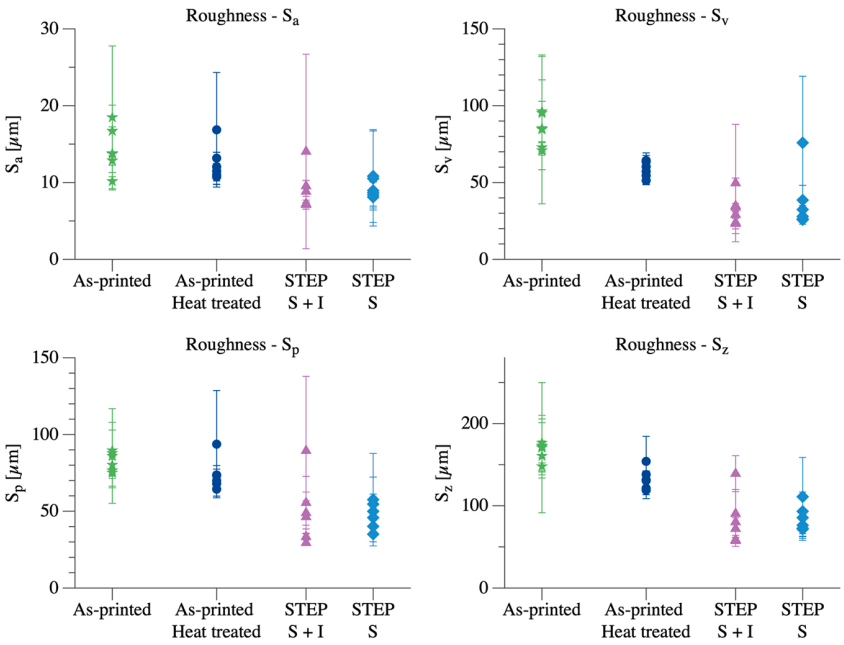

Fig. 9. Plot of areal surface roughness parameters average surface roughness (S_a), average minimum valley depth (S_v), average maximum peak height (S_p), and average maximum height (S_z) from the surface scans of the fatigue samples. The samples without any surface treatment (as-printed and as-printed heat-treated samples) have a higher S_a, S_v, S_p, and S_z than the samples with surface finishing (STEP with sulfur and iodine and STEP with sulfur only). S_v decreased by 55 % from as-printed samples to STEP with sulfur samples. This corroborates the significant contribution of the surface finishing aspect of STEP towards fatigue performance.

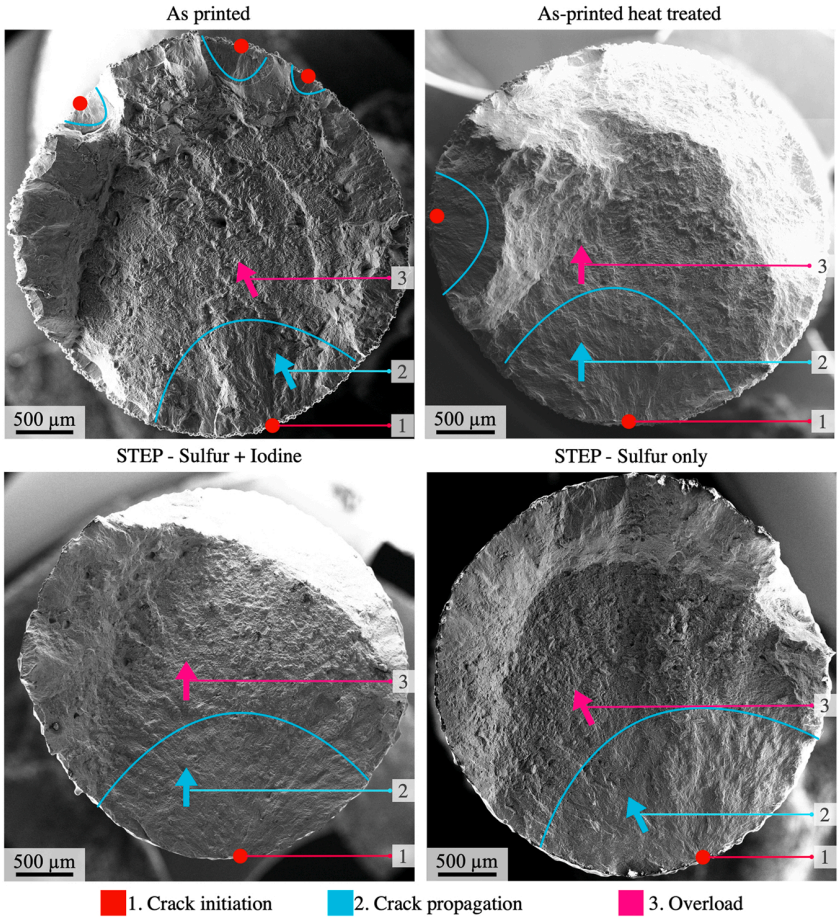

Fig. 10. SEM images of the fracture surfaces of the fatigue specimens with the highest cycles to failure show the crack initiation, crack propagation, and overload regions. The specimens subjected to STEP surface finishing have only one failure initiation point compared to multiple failure initiation points with the as-printed and as-printed heat-treated specimens. Labels 1, 2, and 3 indicate crack initiation, crack propagation, and overload regions respectively.

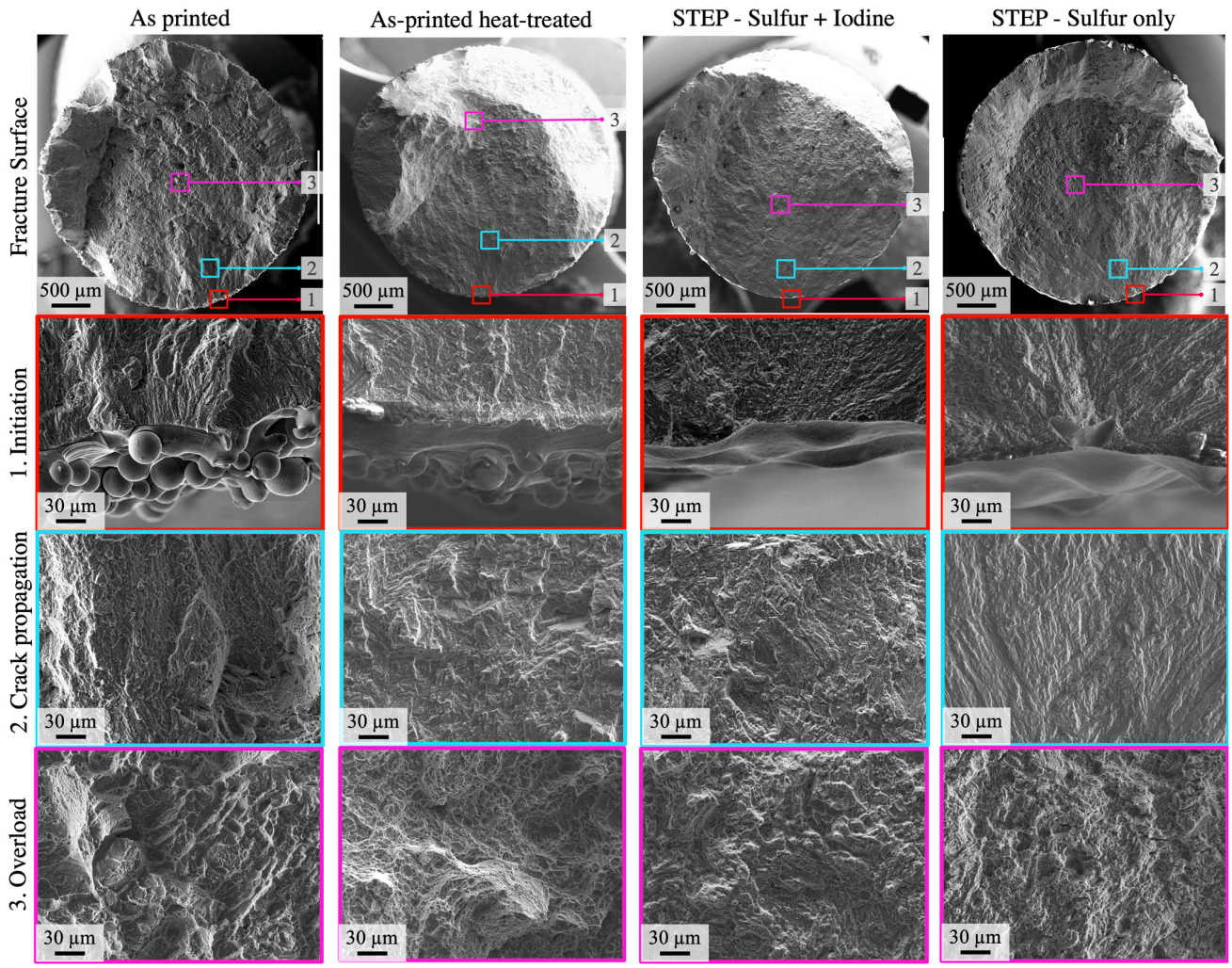

Fig. 11. SEM images of the fracture surfaces of as-printed, as-printed heat-treated, STEP with sulfur and iodine, and STEP with sulfur only fatigue specimens show the respective initiation, crack propagation, and overload regions. The initiation is on the surface for all the specimens, with a more tortuous surface for the as-printed surface than the rest. Labels 1, 2, and 3 indicate crack initiation (second row), crack propagation (third row), and overload (fourth row) regions respectively.

samples, have a higher P_a, although fairly comparable, than the samples subjected to surface finishing, i.e., the STEP with sulfur and iodine and the STEP with sulfur only samples. However, the P_v, P_p, and P_z values of the samples subjected to surface treatment are lower by at least one-third compared to those without any surface treatment, i.e., the depth of notch-like surface irregularities, represented by P_v, has decreased by ~33 % from 37 ± 12 µm for as-printed samples to 25 ± 8 µm for STEP with sulfur samples. P_p and P_z also have decreased by ~33 % from 32 ± 10 µm to 21 ± 8 µm and from 69 ± 14 µm to 45 ± 10 µm respectively for as-printed and STEP with sulfur samples. Therefore, in addition to decreased surface roughness after STEP, the smoothing of sharp radiused features that act as stress concentrations improves the fatigue performance by increasing the resistance to fatigue crack initiation. As expected, there is no significant difference in the roughness parameters between the STEP with sulfur and iodine and STEP with sulfur only since the last two cycles of sulfidation and etching for both the sets of samples were identical.

The areal surface roughness parameters average surface roughness (S_a), average minimum valley depth (S_v), average maximum peak height (S_p), and average maximum height (S_z) were measured from three 650 × 650 µm^2 areas with a laser scanning microscope for each sample. Fig. 9 shows the plot of average values of the areal surface roughness parameters with one standard deviation as error bars for as-printed, as-printed heat-treated, STEP with sulfur and iodine, and STEP with sulfur samples. There is no significant difference in the roughness parameters between the STEP with sulfur and iodine and STEP with sulfur only since the last two cycles of sulfidation and etching for both the sets of samples was identical, as seen earlier with profile analysis. The roughness parameters, S_a, S_v, S_p, and S_z, of the samples without any surface treatment is higher than that of the samples subjected to surface finishing, except for one outlier each in the STEP with sulfur and iodine and STEP with sulfur only samples. S_a decreased by 35 % from 14 ± 3 µm to 9 ± 1 µm, S_v decreased by 55 % from 84 ± 11 µm to 38 ± 19 µm, S_p decreased by 43 % from 83 ± 6 µm to 47 ± 9 µm, and S_z decreased by 49 % from 167 ± 11 µm to 85 ± 15 µm for as-printed and STEP with sulfur samples comparison. The drastic decrease in S_v, that represents the depth of notch-like features, significantly contributed to increase in the fatigue performance by 340 % from as-printed to STEP with sulfur specimens. The lower S_v of as-printed heat-treated samples compared to as-printed could be due to the closing of some micro notches due to expansion of the metal during heat treatment. The trends observed with the areal roughness parameters closely matches that of the profile roughness parameters, which in turn matches the fatigue performance, further corroborating the contribution of the decrease in surface roughness in improving the fatigue performance.

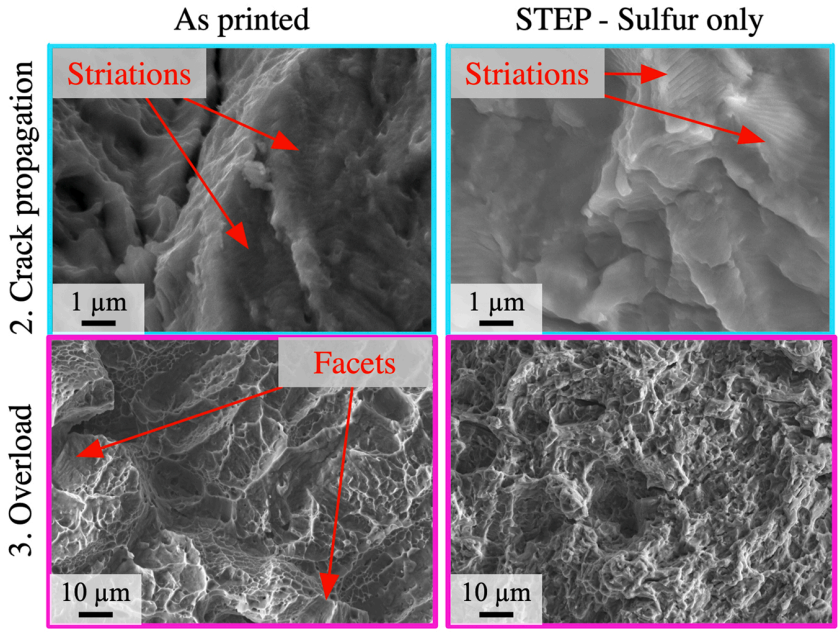

Fig. 12. Higher magnification SEM images of the crack propagation and overload regions of the as-printed and STEP with sulfur fracture surfaces. Ductile striations are visible in both specimens. However, facets in as-printed fracture surface indicate a combination of ductile and brittle failure, whereas in STEP with sulfur, it is mainly ductile.

3.5. *Fracture surface analysis*

Fracture surfaces of the fatigue specimens were analyzed to determine the potential differences in the failure mechanisms between the as-printed, as-printed heat-treated, STEP with sulfur and iodine, and STEP with sulfur specimens. Fig. 10 shows the crack initiation sites, crack propagation, and overload on the fracture surfaces of the specimens with the highest cycles to failure for each specimen process condition. All the fracture surfaces indicate crack initiation at the specimen surface and the end with ductile failure irrespective of their surface roughness and microstructure. The as-printed and as-printed heat-treated specimens, i.e., specimens without any surface finishing, have at least two crack initiation sites compared to one for the specimens subjected to STEP with sulfur and iodine and STEP with sulfur only, i.e., specimens with surface finishing. This is due to the removal of the potential crack initiation sites by improving the surface finish after STEP. The as-printed specimen has more crack initiation sites than the as-printed heat-treated specimen, indicating the microstructural changes and the increase in

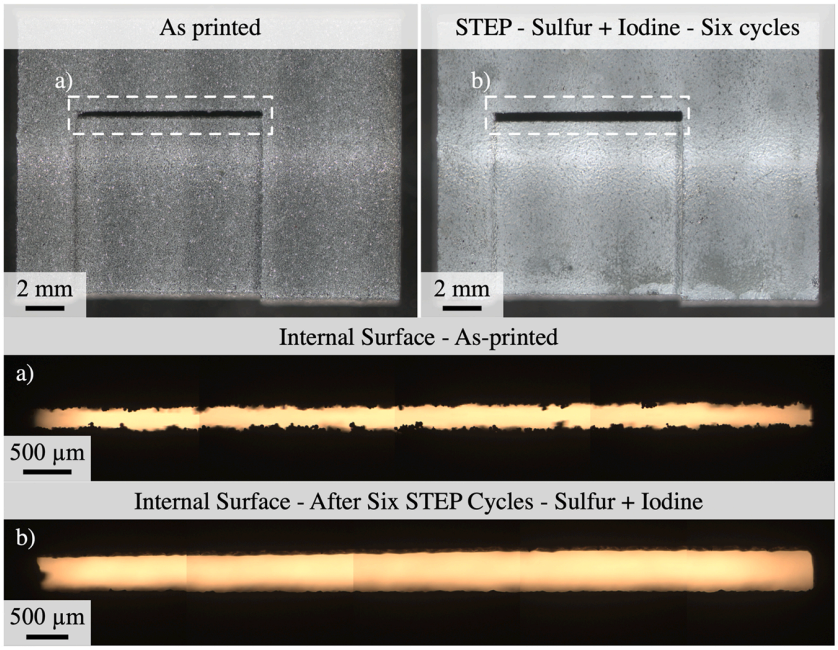

Fig. 13. Optical image of a printed block with an internal surface and a printed block after six STEP cycles with sulfur and iodine. The internal channel width has increased, and the surface irregularities have decreased, leading to a relatively smoother surface.

ductility after the heat treatment make the specimen less sensitive to the surface roughness. Also, notice that the stable crack growth region for the as-printed specimen is significantly smaller than the other specimens.

Fig. 11 shows the SEM images of the initiation, crack propagation, and overload regions of the fracture surfaces of the fatigue specimens with the highest cycles to failure from each set of specimens, i.e., as-printed, as-printed and heat-treated, STEP with sulfur and iodine, and STEP with sulfur only. Failure is initiated at different locations on the surface for all the specimens depending on the depth of the notch-like features and their sensitivity to the cyclic loading, i.e., failure initiates at the largest defect if their shape factor is similar [27]. The fracture surfaces for all the specimens indicate initiation at the surface. The observed surface crack initiation for all the specimens and the number of crack initiation sites indicate that STEP will improve the fatigue performance by decreasing the stress concentration due to surface roughness for a defect-free AM part. The as-printed fracture surface is more tortuous in the fatigue crack propagation region than the rest of the specimens, which could be attributed to the martensitic microstructure and the internal stresses in the as-printed specimens. In addition, the fracture surface appears more jagged in the as-printed fracture surface than in other specimens in the overload region. Fig. 12 shows the higher magnification images of the crack propagation and overload regions of the as-printed and STEP with sulfur fracture surfaces. Ductile striations were observed in both the as-printed and STEP with sulfur fracture surfaces. The presence of facets in the as-printed fracture surface, attributed to the acicular α' microstructure observed in sub-Section 3.3, indicates that the failure is a combination of ductile and brittle failure. In the STEP with sulfur specimen, it is largely ductile failure due to micro void coalescence. Overall, a combination of the surface finishing and microstructural aspects of STEP leads to the enhancement of fatigue performance of AM Ti64 after STEP.

3.6. Demonstration of internal surface finishing

Uniform internal surface finishing is one of the primary advantages of STEP over other post-processing methods. This section demonstrates STEP on a high aspect-ratio internal channel on a printed Ti64 block. First, the printed block is cleaned by sequential sonication in deionized water, acetone, methanol, and isopropyl alcohol for 5 min each, then dried with compressed N_2 gas. Then the block is placed in the tube furnace, and sulfidation with sulfur and iodine is carried out at 750 °C for 12 h and quenched in water with the help of the setup described earlier. Next, the sulfidized block is etched in a solution of 5 M H_2SO_4 and 0.25 M Na_2MoO_4. The sulfidation and etching were repeated five more times, and each cycle increased the internal channel width by about 15–40 μm. The parts need oversizing to account for the material removal to achieve surface finishing. Fig. 13 shows the printed block before and after being subject to six STEP cycles with sulfur and iodine and the side view of the internal surface before and after STEP. The surface finish significantly improved after eliminating surface irregularities on the internal surface. In addition, decreasing the surface roughness of the internal surfaces will decrease the surface crack initiation sites, thereby improving the fatigue performance of printed parts with internal surfaces. This process can be extended to any internal or external surface to improve the surface finish and fatigue performance, provided the surfaces are fluid accessible.

4. Conclusions

We demonstrated a sulfur-based STEP as a post-processing technique to improve the surface finish of AM Ti64, including parts with internal surfaces. STEP with sulfur improved the fatigue cycles to failure by 340 % over the as-printed specimens. The enhanced fatigue performance of the STEP specimens was studied by characterizing the surface roughness, microstructure, and fracture surfaces. The surface finishing from STEP delayed the fatigue crack initiation by decreasing the surface roughness parameter S_v by 55 % from 84 ± 11 μm to 38 ± 19 μm. Furthermore, the transformation of some of the fine acicular α' structures to $\alpha + \beta$ lamellar microstructure during STEP resulted in higher ductility that decreased the sensitivity to surface roughness and increased the resistance to crack propagation. Overall, the fatigue performance improvement is a combined effect of the decrease in surface roughness and the change in microstructure from STEP. Lastly, we demonstrated how these improvements easily extend to internal surfaces with STEP, which is challenging or impossible with other post-processing methods.

CRediT authorship contribution statement

Hildreth Owen J.: Writing – review & editing, Supervision, Resources, Funding acquisition. **Hommer Garrison M.:** Writing – review & editing, Supervision. **Agnani Milan:** Writing – review & editing, Investigation. **Raikar Subbarao:** Writing – review & editing, Writing – original draft, Methodology, Investigation, Formal analysis, Conceptualization. **DiGregorio Steven:** Writing – review & editing, Investigation.

Declaration of Competing Interest

The authors declare that they have no known competing financial interests or personal relationships that could have appeared to influence the work reported in this paper.

Data Availability

Data will be made available on request.

Acknowledgment

Hildreth group gratefully acknowledges the support from the United States Department of Energy under contract agreement Grants #: DE-EE0008166 administered through the Department of Energy's Kansas City National Security Campus, operated by Honeywell Federal Manufacturing & Technologies, LLC, under contract number DE-NA0002839. In addition, we acknowledge the support of Christian Barr at the Kansas City National Security Campus for supplying the printed parts. Finally, we also acknowledge the support from the United States National Science Foundation (CAREER: 1944516).

Appendix A. Supporting information

Supplementary data associated with this article can be found in the online version at doi:10.1016/j.addma.2022.103331.

References

[1] D. Greitemeier, F. Palm, F. Syassen, T. Melz, Fatigue performance of additive manufactured TiAl6V4 using electron and laser beam melting, Int. J. Fatigue 94 (2017) 211–217, https://doi.org/10.1016/j.ijfatigue.2016.05.001.
[2] G. Kasperovich, J. Hausmann, Improvement of fatigue resistance and ductility of TiAl6V4 processed by selective laser melting, J. Mater. Process Technol. 220 (2015) 202–214, https://doi.org/10.1016/j.jmatprotec.2015.01.025.
[3] C.A. Kantzos, R.W. Cunningham, V. Tari, A.D. Rollett, Characterization of metal additive manufacturing surfaces using synchrotron X-ray CT and micromechanical modeling, Comput. Mech. 61 (2018) 575–580, https://doi.org/10.1007/s00466-017-1531-z.
[4] S. Beretta, S. Romano, A comparison of fatigue strength sensitivity to defects for materials manufactured by AM or traditional processes, Int. J. Fatigue 94 (2017) 178–191, https://doi.org/10.1016/j.ijfatigue.2016.06.020.
[5] J. Kranz, D. Herzog, C. Emmelmann, Design guidelines for laser additive manufacturing of lightweight structures in TiAl6V4, J. Laser Appl. 27 (2015) S14001, https://doi.org/10.2351/1.4885235.
[6] S. Pal, G. Lojen, R. Hudak, V. Rajtukova, T. Brajlih, V. Kokol, I. Drstvenšek, As-fabricated surface morphologies of Ti-6Al-4V samples fabricated by different laser processing parameters in selective laser melting, Addit. Manuf. 33 (2020), 101147, https://doi.org/10.1016/j.addma.2020.101147.

[7] H.M. Khan, Y. Karabulut, O. Kitay, Y. Kaynak, I.S. Jawahir, Influence of the post-processing operations on surface integrity of metal components produced by laser powder bed fusion additive manufacturing: a review, Mach. Sci. Technol. 25 (2021) 118–176, https://doi.org/10.1080/10910344.2020.1855649.
[8] G. Annamaria, B. Massimiliano, V. Francesco, Laser polishing: a review of a constantly growing technology in the surface finishing of components made by additive manufacturing, Int. J. Adv. Manuf. Technol. 120 (2022) 1433–1472, https://doi.org/10.1007/s00170-022-08840-x.
[9] P. Jamshidi, M. Aristizabal, W. Kong, V. Villapun, S.C. Cox, L.M. Grover, M. M. Attallah, Selective laser melting of Ti-6Al-4V: the impact of post-processing on the tensile, fatigue and biological properties for medical implant applications, Materials 13 (2020) 2813, https://doi.org/10.3390/ma13122813.
[10] E. Maleki, S. Bagherifard, M. Bandini, M. Guagliano, Surface post-treatments for metal additive manufacturing: progress, challenges, and opportunities, Addit. Manuf. 37 (2020), 101619, https://doi.org/10.1016/j.addma.2020.101619.
[11] A. Fatemi, R. Molaei, S. Sharifimehr, N. Phan, N. Shamsaei, Multiaxial fatigue behavior of wrought and additive manufactured Ti-6Al-4V including surface finish effect, Int. J. Fatigue 100 (2017) 347–366, https://doi.org/10.1016/j.ijfatigue.2017.03.044.
[12] H. Zhang, J. Zhao, J. Liu, H. Qin, Z. Ren, G.L. Doll, Y. Dong, C. Ye, The effects of electrically-assisted ultrasonic nanocrystal surface modification on 3D-printed Ti-6Al-4V alloy, Addit. Manuf. 22 (2018) 60–68, https://doi.org/10.1016/j.addma.2018.04.035.
[13] H. Zhang, R. Chiang, H. Qin, Z. Ren, X. Hou, D. Lin, G.L. Doll, V.K. Vasudevan, Y. Dong, C. Ye, The effects of ultrasonic nanocrystal surface modification on the fatigue performance of 3D-printed Ti64, Int. J. Fatigue 103 (2017) 136–146, https://doi.org/10.1016/j.ijfatigue.2017.05.019.
[14] C.P. Ma, Y.C. Guan, W. Zhou, Laser polishing of additive manufactured Ti alloys, Opt. Laser Eng. 93 (2017) 171–177, https://doi.org/10.1016/j.optlaseng.2017.02.005.
[15] T. Persenot, J.-Y. Buffiere, E. Maire, R. Dendievel, G. Martin, Fatigue properties of EBM as-built and chemically etched thin parts, Procedia Struct. Integr. 7 (2017) 158–165, https://doi.org/10.1016/j.prostr.2017.11.073.
[16] S. Raikar, M. Heilig, A. Mamidanna, O.J. Hildreth, Self-terminating etching process for automated support removal and surface finishing of additively manufactured Ti-6Al-4 V, Addit. Manuf. 37 (2021), 101694, https://doi.org/10.1016/j.addma.2020.101694.
[17] C. Schneider, W. Rasband, K. Eliceiri, NIH Image to ImageJ: 25 years of image analysis, Nat. Methods (2012) 671–675, https://doi.org/10.1038/nmeth.2089.
[18] B. Vrancken, L. Thijs, J.-P. Kruth, J.V. Humbeeck, Heat treatment of Ti6Al4V produced by Selective Laser Melting: Microstructure and mechanical properties, J. Alloy Compd. 541 (2012) 177–185, https://doi.org/10.1016/j.jallcom.2012.07.022.
[19] F.C. Campbell, ed., 2008. Fatigue, Elements of Metallurgy and Engineering Alloys. (2008) 243–264. ⟨https://doi.org/10.31399/asm.tb.emea.t52240243⟩.
[20] S. Leuders, T. Lieneke, S. Lammers, T. Tröster, T. Niendorf, On the fatigue properties of metals manufactured by selective laser melting – The role of ductility, J. Mater. Res. 29 (2014) 1911–1919, https://doi.org/10.1557/jmr.2014.157.
[21] P. Edwards, M. Ramulu, Fatigue performance evaluation of selective laser melted Ti–6Al–4V, Mater. Sci. Eng. 598 (2014) 327–337, https://doi.org/10.1016/j.msea.2014.01.041.
[22] S. Ren, Y. Chen, T. Liu, X. Qu, Effect of build orientation on mechanical properties and microstructure of Ti-6Al-4V manufactured by selective laser melting, Metall. Mater. Trans. 50 (2019) 4388–4409, https://doi.org/10.1007/s11661-019-05322-w.
[23] M. Benedetti, E. Torresani, M. Leoni, V. Fontanari, M. Bandini, C. Pederzolli, C. Potrich, The effect of post-sintering treatments on the fatigue and biological behavior of Ti-6Al-4V ELI parts made by selective laser melting, J. Mech. Behav. Biomed. 71 (2017) 295–306, https://doi.org/10.1016/j.jmbbm.2017.03.024.
[24] A. Yadollahi, N. Shamsaei, Additive manufacturing of fatigue resistant materials: challenges and opportunities, Int. J. Fatigue 98 (2017) 14–31, https://doi.org/10.1016/j.ijfatigue.2017.01.001.
[25] K.S. Chan, M. Koike, R.L. Mason, T. Okabe, Fatigue life of titanium alloys fabricated by additive layer manufacturing techniques for dental implants, Metall. Mater. Trans. 44 (2013) 1010–1022, https://doi.org/10.1007/s11661-012-1470-4.
[26] J. Gockel, L. Sheridan, B. Koerper, B. Whip, The influence of additive manufacturing processing parameters on surface roughness and fatigue life, Int. J. Fatigue 124 (2019) 380–388, https://doi.org/10.1016/j.ijfatigue.2019.03.025.
[27] S. Liu, Y.C. Shin, Additive manufacturing of Ti6Al4V alloy: a review, Mater. Des. 164 (2019), https://doi.org/10.1016/j.matdes.2018.107552, 107552–23.